2013

SIMULATING LARGE DEFORMATION OF INTRANEURAL GANGLION CYST USING FINITE ELEMENT METHOD

Sachin Lokhande
Michigan Technological University

SIMULATING LARGE DEFORMATION OF INTRANEURAL GANGLION CYST USING FINITE ELEMENT METHOD

By

Sachin Lokhande

A REPORT

Submitted in partial fulfillment of the requirements for the degree of

MASTER OF SCIENCE

In Mechanical Engineering

MICHIGAN TECHNOLOGICAL UNIVERSITY

2013

The report has been approved in the partial fulfillment of the requirements for the Degree of MASTER OF SCIENCE in Mechanical Engineering.

Mechanical Engineering – Engineering Mechanics

Report Advisor:	Dr. Gregory Odegard
Committee Member:	Dr. Tolou Shokuhfar
Committee Member:	Dr. Zhanping You
Department Chair:	Dr. William Predebon

TABLE OF CONTENTS:

ABSTRACT

Intraneural Ganglion Cyst is disorder observed in the nerve injury, it is still unknown and very difficult to predict its propagation in the human body so many times it is referred as an unsolved history. The treatments for this disorder are to remove the cystic substance from the nerve by a surgery. However these treatments may result in neuropathic pain and recurrence of the cyst. The articular theory proposed by Spinner et al., (Spinner et al. 2003) considers the neurological deficit in Common Peroneal Nerve (CPN) branch of the sciatic nerve and adds that in addition to the treatment, ligation of articular branch results into foolproof eradication of the deficit. Mechanical modeling of the affected nerve cross section will reinforce the articular theory (Spinner et al. 2003). As the cyst propagates, it compresses the neighboring fascicles and the nerve cross section appears like a signet ring. Hence, in order to mechanically model the affected nerve cross section; computational methods capable of modeling excessively large deformations are required. Traditional FEM produces distorted elements while modeling such deformations, resulting into inaccuracies and premature termination of the analysis. The methods described in research report have the capability to simulate large deformation. The results obtained from this research shows significant deformation as compared to the deformation observed in the conventional finite element models. The report elaborates the neurological deficit followed by detail explanation of the Smoothed Particle Hydrodynamic approach. Finally, the results show the large deformation in stages and also the successful implementation of the SPH method for the large deformation of the biological organ like the Intra-neural ganglion cyst.

1. MOTIVATION:

The articular theory proposed by et al., (Spinner et al. 2003) explains the neurological deficit in Common Peroneal Nerve (CPN) branch of sciatic nerve and affirms that ligation of articular branch results into foolproof eradication of the deficit. This theory is proposed as a solution to the disorder that occurs due to nerve injury called Intraneural Ganglion Cyst (200 year old mystery related to nerve injury, which is yet to be solved)

Current treatments are relatively simple procedures to remove cystic content from the nerve. However, these treatments may result into neuropathic pain and recurrence of the cyst. So the mechanical modeling of the affected nerve cross section will reinforce the articular theory (Spinner et al. 2003).

In this disorder as the cyst propagates, it compresses the neighboring fascicles and the nerve cross section bulges out radially. Hence, in order to mechanically model the affected nerve cross section; computational methods capable of modeling excessively large deformations are required. Traditional FEM produces distorted elements while modeling such deformations, resulting into inaccuracies and premature termination of the analysis.

The basic objective of this research work is to simulate the large deformations observed in biological organs similar to nerves.

The method described in this report is an attempt made to simulate this high deformation.

The result obtained from the model resembles the expansion of the cross section of the nerve.

2. INTRODUCTION:

2.1 Intra Neural Ganglion Cyst (IGC) :

Intraneural Ganglion Cysts is lesions or defects occurring in nerves and causing a neurological deficit. These lesions contain mucin as a primary substance and are believed to be seen around joints. As the name suggests, the cystic lesions occur inside the nerve and as the cyst propagates, the cyst expands due to intra-articular pressures from the joint mechanics and compresses material around it. The material being compressed consists of nerve fascicles and epineurium. Nerve fascicles contain a bundle of nerve fibers enclosed by protective sheathing made up of connective tissue called perineurium. Several such nerve fascicles are bundled together and are surrounded by a layer of connective tissue called epineurium which forms the constituents of a major peripheral nerve.

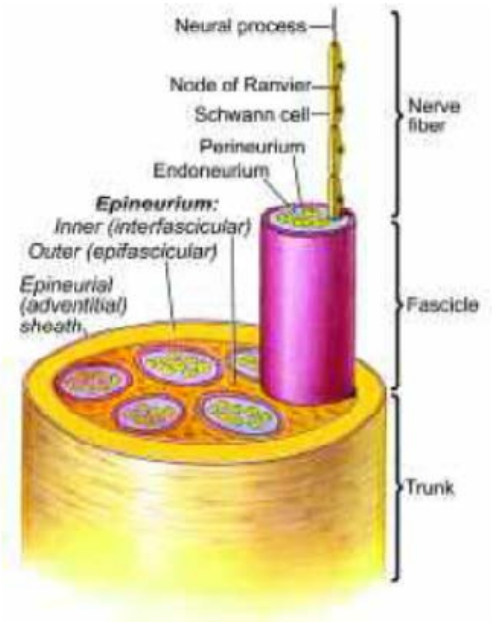

Figure: 1.1-Constituents of major peripheral nerve

As shown in figure 1.1, nerve fascicles contain nerve fibers carrying sensory or motor signals. Hence, compression of these fascicles results in a loss of sensory or motor signal. Current treatments of the problem include removal of cystic contents from the nerve. However, these treatments are not foolproof and result into postoperative recurrence of the defect. These cysts occur at several locations in human body, but are predominantly seen in nerves of the lower leg. Whenever a nerve is mechanically loaded, Epineurial tissue functions as a shock absorber, resulting in dissipation of strain energy set up in the nerve. The dissipation of strain energy increases with increasing amount of Epineurial tissue. Figure 1.2 explains the concept of dissipation of strain energy in nerve having a number of fasciculi supported with Epineurial tissue interspersed in between the fascicles. Because, Common Peroneal Nerve (CPN) division of a sciatic nerve is composed of large and closely packed fasciculi with little supporting Epineurial tissue, it is more susceptible

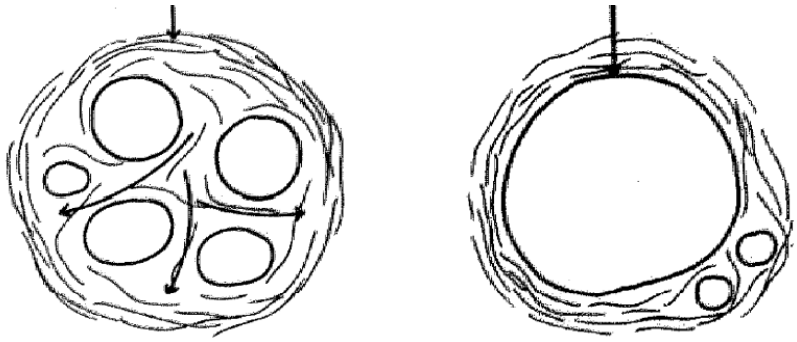

Figure 1.2 Dispersion of Compression stresses by Epineurial tissue

to nerve injury. This work focuses on Intraneural Ganglion Cyst occurring in a CPN division of a sciatic nerve. A unifying theory based on the importance of articular branch in the formation and growth of Peroneal Intraneural Ganglion Cyst (IGC) proposed by Spinner et al., (Spinner et al. 2003) explains the involvement of superior Tibia-fibular joint in the formation of the cyst. The

anatomy of CPN and its branches suggest that articular branch connected to the joint serves as a conduit for synovial fluid (joint fluid) to pass through itself and enter the Common Peroneal Nerve. This aberration occurs due to defects in the joint which may have been previously traumatized, degenerated or congenitally weakened. Due to large intra articular pressures, the articular branch becomes remarkably enlarged and results into formation of IGC.

Figure 2.3 shows the anatomy of the CPN and its branches and path of cyst propagation from articular branch to sciatic nerve. It is believed that the fluid follows the path of least resistance and flows proximally up from articular branch to CPN and finally up to the sciatic nerve depending upon the anatomy of CPN and its nerve branches. Due to defect in the joint, the cyst fluid oozes out from the joint and enters the articular branch. The large intra-articular pressures associated with loading and joint mechanics result in cystic appearance of CPN. The predilection of the cyst to propagate proximally depends on the anatomy of articular branch. For this, anatomical study (R. Spinner et al. 2003) of 20 cadaveric limbs was performed which supports the proximal dissection of the cyst from the articular branch to sciatic nerve. Moreover, to understand the cyst pathogenesis, a dye study (R. Spinner, J. Atkinson, et al. 2003) was performed on five specimens concluding that cyst dissects proximally to the sciatic nerve.

Typically, cyst propagation is categorized into four stages:

Stage I: Cyst fluid flows in the articular branch resulting into mechanical pain.

Stage II: Cyst fluid crosses the trifurcation of the articular branch, DPN and superficial branches resulting in neuropathic pain and neurological deficit in DPN.

Stage III: Cyst fluid enters CPN resulting into motor nerve weakness.

Stage IV: Dissection extends proximal to sciatic nerve bifurcation and enters sciatic nerve resulting into motor and sensory nerve disturbance.

During cyst propagation, cystic fluid under intra-articular pressures compresses the fascicles around it and after reaching Stage IV, simulates an appearance of signet ring. The term 'signet ring sign' was coined by Spinner et al., (Spinner et al. 2006) due to resemblance of MRI image and signet ring.

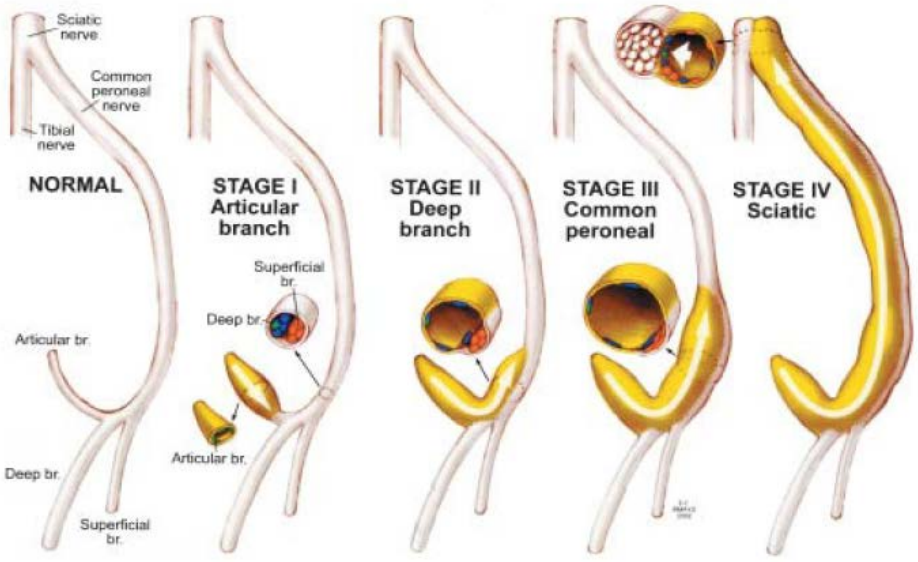

Figure 1.3 Composite Drawing showing the stages of intra-neural ganglia.

The excessive deformation of fascicles leads to neuropathic pain and loss of motor weakness and/or sensory disturbance. A retrospective study of patients suffering from neuropathic pain and presumably the problem of IGC was done on 16 cases.

3. Limitations of Finite Element Analysis (FEA) in Biomechanics:

Biomechanics is a field of engineering which deals with mechanics of biological materials. Biological materials fall in the class of materials showing inconsistent material behavior in different directions under mechanical loading. Biomechanics involves knowledge of geometry, mechanical properties involved, governing natural laws, mathematical formulation of specific problems, their solutions and validation.

FEM as a concept is a simplification, FEM in Biomechanics also depends on a number of simplifications and assumptions (Gallagher et al. 2006). However, appropriate simplification is a key to good modeling and these appropriate simplifications depend on the hypothesis of the behavior of the system being tested in the model. In general, FEM in Biomechanics has three different aspects:

i. Geometric representation
ii. Material representation (constitutive laws)
iii. Boundary conditions (loading and restraints)

FEM is performed differently in different biological materials namely orthopedic materials, Soft tissues, Bio-fluids etc. as these materials behave differently under mechanical loading. This work mainly focuses on a biological defect involving the mechanics of nervous tissue (soft tissue) and finite element modeling of the cross section of the affected nerve at the fibular neck to resemble it with MRI image obtained at the same location.

4. Application of Finite Element Analysis for large deformations:

The primary constraint in finite element modeling of IGC is excessively large deformation (greater than 100% strain) of neighboring fascicles due to cyst expansion. Traditional FEM suffers from problems like excessive element distortions resulting in inaccuracies and premature termination of analyses while modeling such deformations. Hence, special numerical techniques are required to model such large deformations. Research conducted at University of Pittsburgh by Sidorov, is based on finite element modeling of Aneurysm development and growth which is similar to modeling IGC propagation. Here, finite element modeling of Balloon Angioplasty and Fusiform Aneurysm were performed in commercial code Ansys using a multi-mechanism inelastic material model. However, this research was mainly concerned with the observation of stresses at the fully affected aneurysm sites and not with propagation of Aneurysms from its unaffected state to affected state.

Dheeranvongkit and Shimada (Dheeravongkit & Shimada 2005) maintained the shape quality of elements during large deformation by gaining knowledge about the final deformation boundary and stress state. Then, re-meshing of the final deformation boundary was performed to control the mesh shapes and sizes. Finally, mapping of the element was done to un-deformed configuration by inverse bilinear mapping. Due to which, the shape quality of elements was preserved throughout the deformation.

To model such large deformations, advanced techniques are required to prevent mesh distortions and inaccuracies. Also, there is additional complexity to model biological materials with governing material non linearity and directionality characteristics. Meshless methods are considered as techniques which are capable of modeling excessively large deformations. Due to

absence of the mesh, the problem of mesh distortions is avoided and also the computational time and cost due to re-meshing techniques is also saved.

Meshless methods were used in biological applications to study the effect of soft tissue deformations during surgical simulations by Horton et al., (Horton et al. 2007). In their study, the Element Free Galerkin Method (EFGM) was used to obtain reaction forces at nodes on the contact surface of a swine brain by assigning prescribed displacements to a set of nodes. A cloud of nodes were used to discretize the problem domain and background cells were used to obtain system matrices. Results obtained were fairly accurate and validated well with the experimental results.

Doblare et al., (Doblare et al. 2004) was another group of researchers that made use of Meshless methods in biomechanics. They used the Natural Element Method (NEM) for simulation of adaptive bone remodeling. NEM prevented the formation of checkerboard phenomenon, which was considered to be the main drawback of FEM while modeling bone tissue adaptation. The values of density distribution at the femoral neck and head closely matched with the actual radiographic images of the femur after similar time steps.

Meshless methods are also capable of modeling large deformations in Hyperplastic materials. This type of work was conducted by Kawashima and Sakai, (Kawashima & Sakai 2007). They used Smooth Particle Hydrodynamics (SPH) which is a form of Meshless modeling for analyzing large deformations of rubber. SPH was used to simulate the experimental setup of elastic sealant indentation test. Here, a cylindrical material was pushed into an elastic sealant made of polymer resulting into excessive deformations of the sealant. Traditional FEM may result in mesh distortions, leading to inaccuracies or premature termination of the analysis due to

large deformation of the elastic sealant. However, due to absence of mesh, SPH was able to simulate the problem with fairly good accuracy.

Due to esoteric nature of Meshless methods, very little is known about different types of mesh less methods and hence, there are a few commercial software packages namely LS-Dyna, Pam Crash, MFree 2D etc. capable of analyzing problems using meshless methods. Another method dealing with large deformation analysis is the Eulerian Finite Element (FE) approach which minimizes element distortions and inaccuracies associated with the classical Lagrangian approach.

Generally, the Eulerian FE approach is used to simulate fluid flow problems. Benson (Benson 1992), Gadala and Wang (Gadala & Wang 1998) first made use of the Eulerian FE approach for simulating excessively large deformations in solids in metal forming, extrusion and die forging applications. This Eulerian FE approach was used by Raczy (Raczy et al. 2004) to simulate deformation state of Copper subjected to orthogonal cutting. They used LS-Dyna for applying the Eulerian technique to study the excessive deformation of copper during the machining process. The strains obtained were of the order of 500 to 600 percent. The results validated well with the experimental local stress and strain values.

A detailed study involving Eulerian FE approach and meshless methods was done by Lee (Lee et al. 2005). They studied the effect of dynamic pressure loading on aorta using advanced numerical techniques. Dynamic pressure resulted in excessive strains in the aorta wall and the formation of vortices in the fluid flowing through aorta. They employed Lagrangian, Arbitrary Lagrangian Eulerian (ALE), Eulerian and SPH formulations to simulate the problem. Stresses, strains and velocity of fluid were obtained as output parameters. Comparison of output

parameters from each method concluded that SPH gave better results concerning idealized fluid flow, but the Eulerian approach gave fairly accurate results concerning the deformation of aorta wall.

Work related to FE modeling of Intraneural Ganglion Cyst (IGC) was performed by Elangovan, (Elangovan et al. 2009) and (Elangovan 2010). They categorized the IGC propagation into two stages. Stage I considered the propagation of IGC in the articular branch. Modeling of Stage I was performed using a 3 dimensional FE model. Stage II considered the propagation of IGC in Common Peroneal Nerve (CPN) division of the sciatic nerve. Modeling of Stage II was performed using a 2 dimensional FE model. The approach for modeling cyst propagation in both the stages was based on a combined geometrical and physical growth criterion (Huang and Black 1996). In this approach, element separation was performed when the stress value of an element exceeded failure strength of that particular material. However, application of this approach approximates propagation of the cyst by failure of neighboring fascicles rather than propagation of cyst by actual deformation of fascicles. The primary constraint involved in modeling of this neurological deficit is the excessively large deformations of fascicles due to expansion of IGC. Hence, a computational method capable of modeling such large deformations is required to model this neurological deficit.

5. Objective:

The primary objective of this research is to mechanically model the growth and propagation of Intraneural Ganglion Cyst in CPN division of Sciatic nerve by using a two dimensional finite element model by actual deformation of fascicles (elements). This research mainly focuses on the advanced numerical techniques used to model the cross section of affected CPN at the fibular neck, simulating propagation of the cyst from Stage I to Stage IV (depicted in figure 1.3) to resemble it with MRI image of the affected CPN cross section at the same location. Strain due to deformation of fascicles during cyst growth from Stage I to Stage IV in CPN cross section is expected to be greater than 100%. Hence, advanced numerical techniques capable of modeling strains greater than 100% are required to simulate cyst propagation.

This report focuses on meshless method/techniques capable of modeling excessively large deformations using SPH: Smoothed Particle Hydrodynamic approach

6. FEA Model creation of affected CPN cross-section:

Sunderland and Ray, (Sunderland & Ray 1948) investigated the behavior of fascicles and its intra-fascicular mixing forming intra-neural plexus formations. For this, they prepared histological sections from segments of sciatic nerve between sciatic notch and tibia malleolus from 40 adult subjects. The sections were enlarged, drawn and arranged in a serial fashion. Thus, several drawings of cross sections of a sciatic nerve were prepared at different locations. The drawing of the nerve cross section at the fibular neck was of primary interest. Figure 6.1 shows the drawing of the cross section of the nerve at fibular neck. According to Spinner et al., 2003, it was believed that cysts arise from the articular branch. The articular branch is located eccentric to the left in the drawing represented by 'G' shown in figure 6.1. Hence, the cyst in the form of a circular through hole was located in the model eccentric to the left representing the articular branch.

A finite element model was created in Abaqus 6.9 and the cyst arising from articular branch was treated as a hole. The geometry of the outer boundary of the model was scanned and imported in Abaqus 6.9. The dimensions of the FE model were calculated by scaling the model according to the image obtained in Figure 6.1. The major axis of the ellipse 'a' as shown in figure 6.2 was obtained by experimental data obtained from Spinner et al., 2007 and was 5.7 mm.

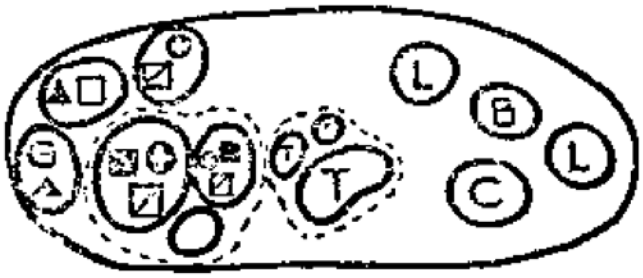

Figure 6.1 Schematic drawing cross section of the CPN

The minor axis ‘b’ of the ellipse was obtained by equation.

$$\frac{\text{Major axis obtained from figure 2.1}}{\text{Minor axis obtained from figure 2.1}} = \frac{\text{Major axis ‘a’ in FE Model}}{\text{Minor axis ‘b’ in FE Model}}$$

The minor axis obtained from the above relation was equal to 2.52 mm. Figure 6.2 shows the finite element model of the affected CPN cross section at fibular neck. Due to lack of initial guiding data, the diameter of the cyst was considered to be 0.18 mm. This dimension locates the cyst within the fascicle boundary. Since, intra-articular pressures were responsible for propagation of the cyst; the hole was subjected to internal pressure in radial outward direction to simulate the propagation of the cyst from Stage I to Stage IV.

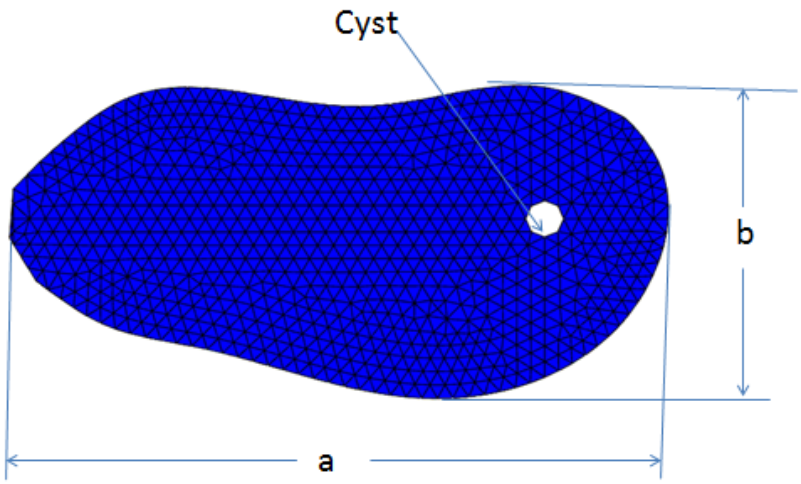

Figure 6.2 Finite Element model of affected CPN at fibular neck

7. Material properties and its assumptions:

In order to model the Nerve Cross section for cyst blow out, oval shapes were to be assigned fascicle properties and epineurium material properties to the area interspersed in between the oval shapes shown in figure 6.1. However, large complexities were involved in maintaining the boundaries between fascicle and epineurium during excessive deformation. Hence, for modeling simplicity, the entire area inside the boundary of the nerve was assumed to be a homogenous continuum. Moreover, fascicles and epineurium are anisotropic materials having nonlinear material behavior. Material non linearity creates convergence issues while modeling such large deformations. In addition, incompressibility associated with soft tissues creates further complexities in obtaining an accurate solution. The objective of this research is to mechanically model the propagation of ganglion cyst at an affected nerve cross section. Hence, strains are of primary importance in this research. Strains are obtained by differentiating displacements calculated from the numerical solution. Material models are involved only in calculation of stresses. Therefore, the assumption of using a linear elastic material having Elastic modulus similar to the nerve material can be conveniently made in this case.

Elastin and collagen are the major constituents of nerve material and approximately have a linear elastic behavior. Wu et al., 2004 obtained the longitudinal elastic modulus of elastin, cured elastin and native carotid artery by testing dumbbell shaped specimens in tension. Native carotid artery has elastin and collagen as its primary constituents. Hence, Properties of native carotid artery were approximated to be similar to the material properties of CPN. Average Elastic modulus of native carotid artery measured in the experiment was E = 4.6 MPa. Mass Density of human patellar tendon was measured by Hashemi et al. (Hashemi, Chandrashekhar and

Slauterback 2005) and equal to $\rho = 0.76$ g/cm^3. Since, human patellar tendon contains elastin and collagen as its primary constituents. CPN was assigned a compressible linear elastic material property having $\rho = 7.6 \times 10^{-7}$ kg/mm^3; E = 4.6 MPa and $\nu = 0.3$.

Thus, the finite element model was subjected to boundary conditions and loads in order to simulate a cyst blow out at the fibular neck which is discussed in further sections.

8. **Mesh-less Methods** (also known as Mesh free Methods):

In the field of numerical simulation methods, the **meshfree methods** are those which do not require a predefined mesh connecting the data points of the simulation domain. Meshfree methods enable the simulation of some otherwise difficult types of problems, at the cost of extra computing time and programming effort.

8.1 **Motivation for mesh-less method**:

Numerical methods such as the finite difference method, finite-volume method, and finite element method were originally defined on meshes of data points. In such a mesh, each point has a fixed number of predefined neighbors, and this connectivity between neighbors can be used to define mathematical operators like the derivative. These operators are then used to construct the equations to be simulated, such as the Euler equations or the Navier–Stokes equations.

But in simulations where the material being simulated can move around (as in computational fluid dynamics) or where large deformations of the material can occur (as in simulations of plastic materials), the connectivity of the mesh can be difficult to maintain without introducing error into the simulation. If the mesh becomes tangled or degenerate during simulation, the operators defined on it may no longer give correct values. The mesh may be recreated during simulation (a process called remeshing), but this can also introduce error, since all the existing data points must be mapped onto a new and different set of data points. The meshfree methods are intended to remedy these problems.

Meshfree methods are also useful for:

- Simulations where creating a useful mesh from the geometry of a complex 3D object may be especially difficult or require human assistance
- Simulations where nodes may be created or destroyed, such as in cracking simulations
- Simulations where the problem geometry may move out of alignment with a fixed mesh, such as in bending simulations
- Simulations containing nonlinear material behavior, discontinuities or singularities

9. **SPH : Smoothed Particle Hydrodynamic method:**

Smoothed particle hydrodynamics (SPH) is a numerical method that is part of the larger family of mesh-less methods. This methods you do not define nodes and elements as you would normally define in a finite element analysis; instead, only a collection of points are necessary to represent a given body. In smoothed particle hydrodynamics these nodes are commonly referred to as particles.

Smoothed particle hydrodynamics is a Lagrangian modeling allowing the discretization of a prescribed set of continuum equations by interpolating the properties at a discrete sets formed by points distributed over the solution domain eliminating the requirement to define a spatial mesh. The method's Lagrangian nature, associated with the absence of a fixed mesh, is its main strength. Difficulties associated with fluid flow and structural problems involving large deformations and free surfaces are resolved in a relatively natural way. From the beginning the method has received theoretical support (Gingold and Monaghan, 1977), and the number of publications related to the method is now very large. A number of references are listed below.

At its core, the method is not based on discrete particles (spheres) colliding with each other in compression or exhibiting cohesive-like behavior in tension as the word particle might suggest. Rather, it is simply a clever discretization method of continuum partial differential equations. In that respect, smoothed particle hydrodynamics is quite similar to the finite element method.

The method can use any of the materials available in Abaqus/Explicit (including user materials). You can specify initial conditions and boundary conditions as for any other Lagrangian model.

Contact interactions with other Lagrangian bodies are also allowed, thus expanding the range of applications for which this method can be used.

9.1 **SPH with illustration**:

In a traditional finite difference simulation, the domain of a one-dimensional simulation would be some function $u(x,t)$, represented as a mesh of data values u_i^n at points x_i, where

$$i = 0, 1, 2...$$

$$n = 0, 1, 2...$$

$$x_{i+1} - x_i = h \ \forall i$$

$$t_{n+1} - t_n = k \ \forall n$$

We can define the derivatives that occur in the equation being simulated using some finite difference formulae on this domain, for example

$$\frac{\partial u}{\partial x} = \frac{u_{i+1}^n - u_{i-1}^n}{2h}$$

and

$$\frac{\partial u}{\partial t} = \frac{u_i^{n+1} - u_i^n}{k}$$

Then we can use these definitions of $u(x,t)$ and its spatial and temporal derivatives to write the equation being simulated in finite difference form, then simulate the equation with one of many finite difference methods.

In this simple example, the spatial step size h and the temporal step size k are constant, and the left and right mesh neighbors of the data value at x_i are the values at x_{i-1} and x_{i+1}, respectively. But if the values can move around, or can be added to or removed from the simulation that destroys the spacing and the simple finite difference formulae for derivatives will no longer be correct.

Smoothed-particle hydrodynamics (SPH), one of the oldest meshfree methods, solves this problem by treating our data points as physical particles with mass and density which can move around over time, and which carry some value u_i with them. SPH then defines the value of $u(x,t)$ between the particles by

$$u(x,t_n) = \sum_i m_i \frac{u_i^n}{\rho_i} W(|x - x_i|)$$

where m_i is the mass of particle i, ρ_i is the density of particle i, and W is a kernel function that operates on nearby data points and is chosen for smoothness and other useful qualities. By linearity, we can write the spatial derivative as

$$\frac{\partial u}{\partial x} = \sum_i m_i \frac{u_i^n}{\rho_i} \frac{\partial W(|x - x_i|)}{\partial x}$$

Then we can use these definitions of $u(x,t)$ and its spatial derivatives to write the equation being simulated as an ordinary differential equation, and simulate the equation with one of many numerical methods. In physical terms, this means calculating the forces between the particles, then integrating these forces over time to determine their motion.

The advantage of SPH in this situation is that the formulae for $u(x,t)$ and its derivatives do not depend on any adjacency information about the particles; they can use the particles in any order, so it doesn't matter if the particles move around or even exchange places.

One disadvantage of SPH is that it requires extra programming to determine the nearest neighbors of a particle. Since the kernel function W only returns nonzero results for nearby particles within twice the "smoothing length" (because we typically choose kernel functions with compact support). It would be a waste of effort to calculate the summations above over every particle in a large simulation. So typically SPH simulators require some extra code to speed up this nearest neighbor calculation.

9.2 **Applications of SPH method** :

Smoothed particle hydrodynamic analyses are effective for applications involving extreme deformation. Fluid sloshing, wave engineering, ballistics, spraying (as in paint spraying), gas flow, and obliteration and fragmentation followed by secondary impacts are a few examples. There are many applications for which both the coupled Eulerian-Lagrangian and the smoothed particle hydrodynamic methods can be used. In many coupled Eulerian-Lagrangian analyses the material to void ratio is small and, consequently, the computational effort may be prohibitively

high. In these cases, the smoothed particle hydrodynamic method is preferred. For example, tracking fragments from primary impacts through a large volume until secondary impact occurs can be very expensive in a coupled Eulerian-Lagrangian analysis but comes at no additional cost in a smoothed particle hydrodynamic analysis.

9.3. Model creation:

To create a part a 3D modeling space is defined because SPH dynamic explicit analysis cannot be done using 2D planar space and since the geometry is not axis symmetric so Axis-symmetric space is also not chosen.

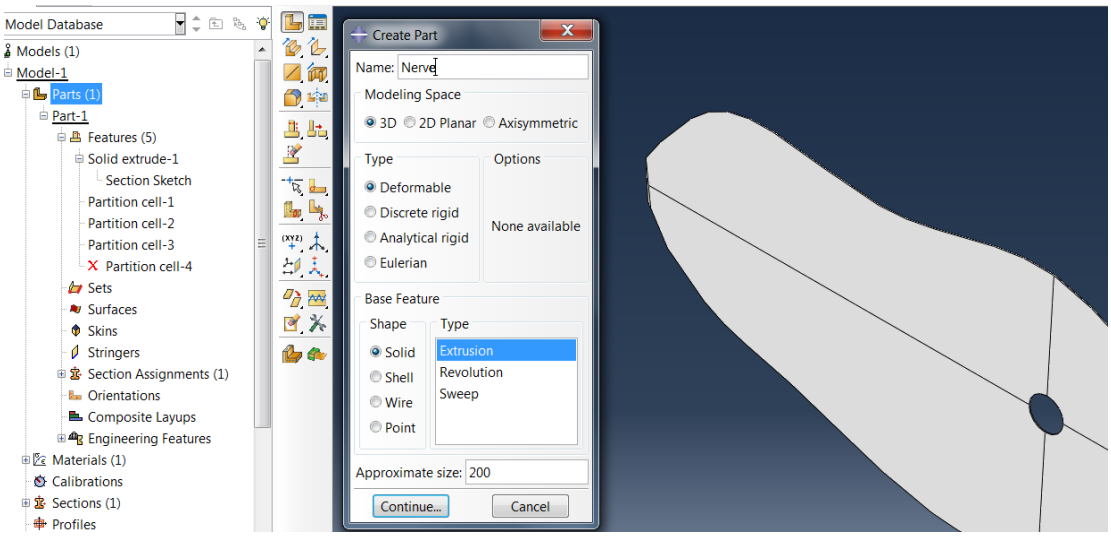

Figure :9.3.1-Parameters for part creation

To perform this analysis a ‘deformable’ type part is chosen.

Eulerian model is good option for the application of pressure boundary conditions but since with the pressure boundary condition it is not possible to convert the domain of element nodes to that of particles, the option of having Eulerian model is also eliminated.

The base feature is selected as per the nature of the part i.e. since the Nerve is a solid extruded part the shape is chosen as solid and the type as extrusion.

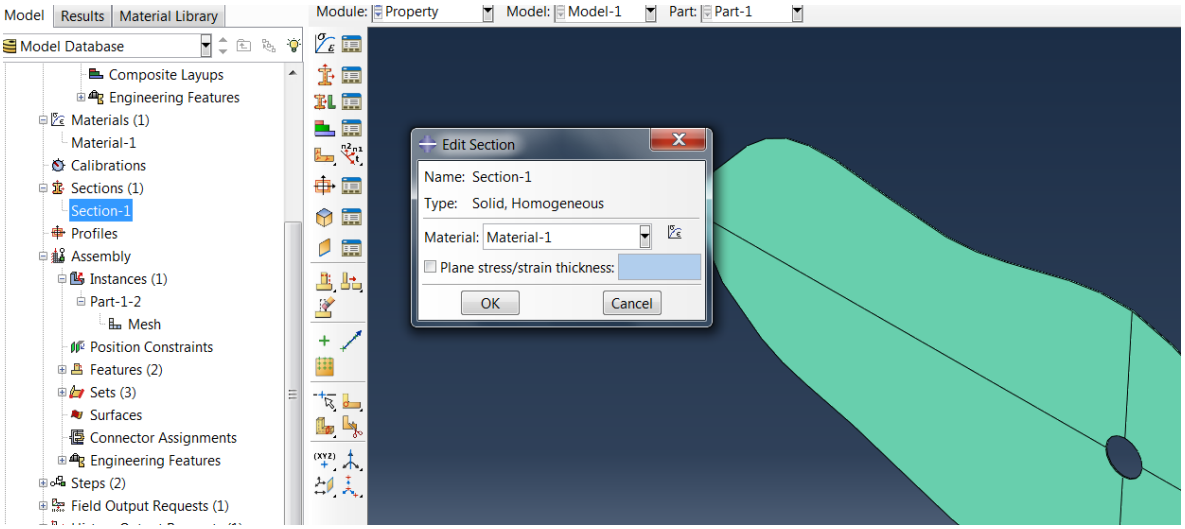

Figure:9.3.2- Material assignment

Section is assigned to the geometry of the cross section of the nerve and the type as a solid homogeneous.

Material as discussed in the section has Young's modulus as 4.6 MPa and ν = 0.3

An independent instance is created in the assembly to mesh the part.

Before meshing the part is partitioned into four quadrants for a uniform meshing near and around the cyst. A tetrahedron mesh is so chosen to have a better accuracy with the results.

Local seeding is done with the Size method and having the size control over the element as 0.3 and curvature control for maximum deviation factor i.e. height to length ratio as 0.1 and minimum size factor as 0.1

9.4. Elements in SPH:

The smoothed particle hydrodynamic method is implemented via the formulation associated with PC3D elements. These 1-node elements are simply a means of defining particles in space that model a particular body or bodies. These particle elements utilize existing functionality in Abaqus to reference element-related features such as materials, initial conditions, distributed loads, and visualization.

These elements are defined in a similar fashion as you would define point masses. The coordinates of these points lie either on the surface or in the interior of the body being modeled, similar to the nodes of a body meshed with brick elements. For more accurate results, strive to space the nodal coordinates of these particles as uniformly as possible in all directions.

As defining each and every co-ordinates for the particles is a laborious job and also as many times the parts are not having a standard shape, another approach is adopted in this research report.

9.5. Conversion of elements to particles:

An advantage of the intrinsic strengths of both Lagrangian finite element and SPH method is taken here when modeling a body. The model is defined with Lagrangian finite elements and converted them to SPH particles either at the beginning of an analysis. It is sometimes easier to create the mesh with Lagrangian finite elements, and Lagrangian finite elements are often more accurate for small deformations. SPH methods are well suited for large deformation.

The analysis is started by defining the part as usual. The part can be meshed with the C3D8R, C3D6, or C3D4 reduced-integration elements or a combination of these elements. Here the part is meshed with the C3D4 elements. Then these "parent" elements can be specified to convert to internally generated SPH particles when a user-specified criterion is met. (The user specified criteria is described in the next section). Gravity loads, contact interactions, initial conditions, mass scaling, and output requests associated with the parent elements or nodes of the parent elements are transferred appropriately to the generated particles upon conversion in an intuitive way as explained below. A special formulation is used to ensure the smoothest possible transition between the two modeling methods.

The element conversion to particles functionality is not active by default. The conversion functionality is intentionally used when the deformations in the original finite element mesh were significant and elements had been distorted. Traditionally, in such cases deletion of the soon-to-be distorted Lagrangian elements would be the only choice to allow the analysis to continue. Converting to SPH particles offers an improvement over the element deletion option because the generated particles are able to provide resistance to deformation beyond finite element distortion levels. Consequently, element deletion cannot be used together with element conversion. The number of particles generated per parent element can be controlled and the conversion into particles can be done by applying different criteria of conversion.

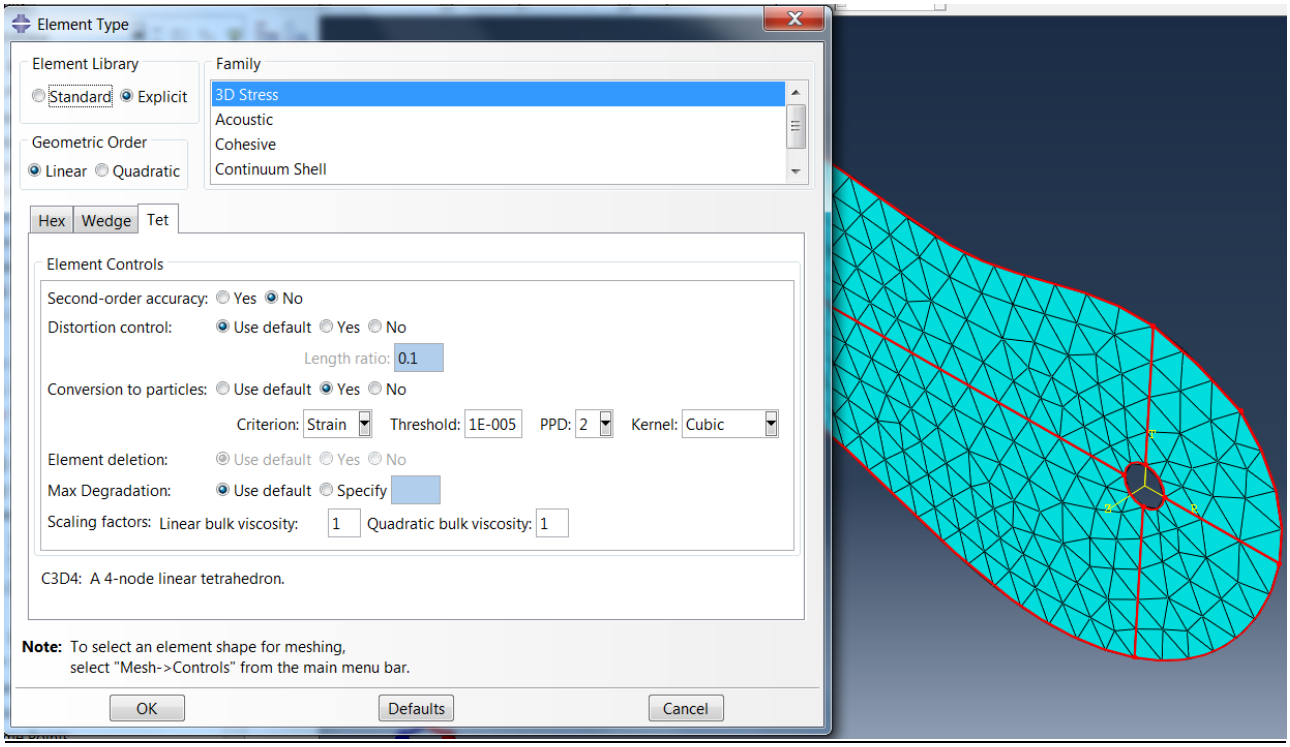

Figure :9.5.1- Particle conversion parameters

Specification of number of particles to be generated:

By default, one particle is generated per parent element. The number of particles generated per element can be controlled by specifying the number of particles to be generated per parent element in iso-parametric direction. The total number of particles generated per element depends on the element type that is being converted. For example, we specify 3 particles to be generated per iso-parametric direction, upon conversion 27 particles would be generated from a C3D8R element, 18 from a C3D6 element, and 10 from a C3D4 element, as illustrated in figure below.

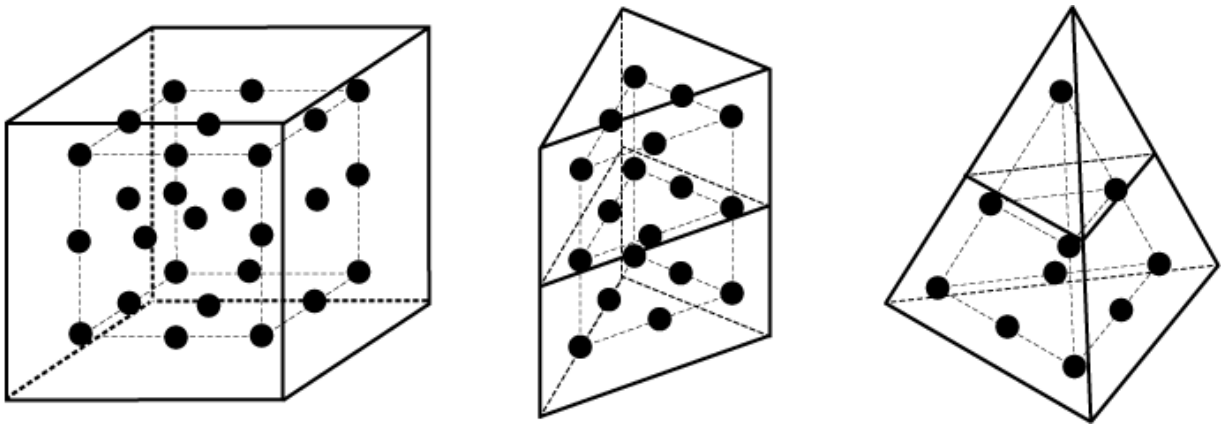

Figure: 9.5.2- Particles per Isoperimetric direction

A maximum value of seven particles per direction can be specified. The particles are evenly spaced inside the parent element such that they fill the volume as uniformly as possible. For example, if cubic parent elements are stacked in the user-defined mesh, the particles would be evenly spaced throughout the part.

Internally generated particles per parent element illustrated for three particles per isoparametric direction.

10. DIFFERENT CRITERIA FOR SPH APPLICATION

10.1. Time based criteria:

You can specify the time when the conversion of all the elements in the affected element set is to take place regardless of the deformation levels. This option is intended for applications where the SPH functionality is the preferred modeling method, such as fluid sloshing in a tank or a synthetic bird strike on an aircraft. If the conversion time is specified as zero, the conversion takes place at the beginning of the analysis. For example, fluid sloshing is a good candidate for using a time-based criterion if sloshing is expected to start at the beginning of the analysis. You can specify a later time at which the conversion takes place if extreme deformations do not occur until later in the analysis. A bird strike analysis is a potential candidate as the bird might travel for some time without any deformation prior to hitting the intended target.

10.2. Strain based criteria:

You can specify the absolute value of the maximum principal strain when the conversion of a given element is to take place. As elements deform, if the absolute value of the maximum strain is greater than the specified threshold, the parent elements will convert progressively to SPH particles. This option is intended for applications where the finite element method is the preferred modeling method but severe deformations could occur in certain regions. Examples include blast applications and crushing.

10.3. Stress based criteria:

You can specify the absolute **v**alue of the maximum principal stress value at which the conversion of a given element takes place. As elements deform, if the absolute value of the maximum principal stress is greater than the specified threshold, the parent elements will convert progressively to SPH particles. This option is intended for the same candidate applications as those discussed for the strain-based criterion.

Conversion to particles formulation:

When using the conversion technique, particles are generated internally at the beginning of the preprocessing phase of the analysis, and they are placed in an inactive or dormant state. The particles are attached to the parent elements in a similar fashion as the nodes of embedded elements are attached, and they follow the motion of the parent element nodes in an average sense. The inertial properties of the particles in this inactive state (while the parent finite elements are active) are automatically disregarded to avoid doubling the momentum at a given location. Similar to SPH particles defined directly as PC3D elements, particles generated from parent element sets associated with different section definitions will not interact with each other.

Upon conversion a number of internally generated particles per parent element are activated, as illustrated for various element types in Figure 15.1.2–1. The computational cost of the analysis can increase significantly after conversion takes place if a large number of particles are generated per element since a larger number of active elements needs to be processed. In addition, the computational cost increases because the stable time increment associated with the internally generated particles decreases as the particle density increases.

Upon conversion the state information (such as stress or equivalent plastic strain) associated with the element being converted is transferred to the generated particles to ensure the smoothest possible transition. The activated particles will interact via the SPH formalism with both the previously activated particles and the neighboring inactive particles that are still embedded in active parent elements.

11. SPH Kernel interpolator:

The interpolation polynomial used for this mesh-less method implemented in Abaqus /Explicit is Cubic spline. There also options using quadratic and quintic interpolator.

The SPH method works on the local interpolations on surrounding particles to construct continuous field approximations. This is the basis for the spatial discretization of governing equations. The interpolation of the value of a function *A* for any position **r** can be expressed using SPH smoothing as proposed by

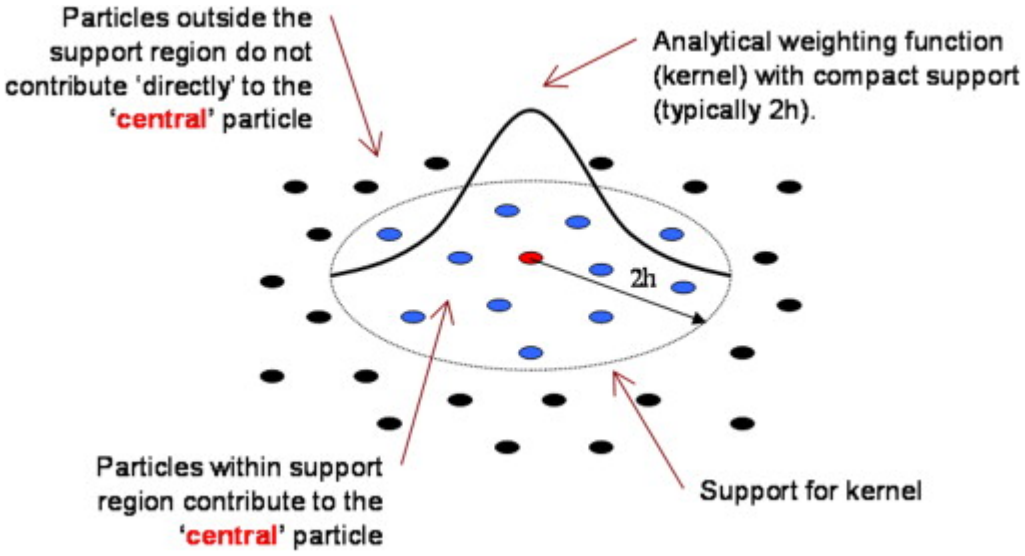

Figure : 11.1 Kernel Function in SPH

$$A(\mathbf{r}) = \sum_b m_b \frac{A_b}{\rho_b} W(\mathbf{r}-\mathbf{r}_b, h)$$

where *mb* and *ρ*b are the mass and the density particle *b*, and the sumation is over all the particles *b* within a radius 2*h* of **r**. Here *W*(**r**, *h*) is a *C*2 the smoothing kernel with radius 2*h*, that gives the approximation of the shape of a Gaussian function with following properties:

$$\int W(|r-r'|,h)\,dr' = 1$$

In the above given limit of integral, the smoothing function approximates a delta function

$$\lim_{h\to 0} W(|r-r'|,h) = \delta(|r-r'|)$$

The kernel in this method has compact support, i.e. it extends with non-zero values up to the limit of radius 2, and has zero value beyond. The kernel is graphically represented as in figure above. The h value depends on the spacing between particles, and is taken as 1.2 times the spacing in particle.

The function can in different types. The cubic kernel is represented as follows:

$$W(u) = \begin{cases} \frac{2}{6}(4-6u^2+3u^3) & \text{if} \quad 0 \le u < 1 \\ \beta(2-u)^3 & \text{if} \quad 1 \le u < 2 \\ 0 & \text{if} \quad u \ge 2 \end{cases}$$

Smoothening length calculation:

Even though particle elements are defined in the model using one node per element, the smoothed particle hydrodynamic method computes contributions for each element based on neighboring particles that are within a sphere of influence. The radius of this sphere of influence is referred to in the literature as the smoothing length. The smoothing length is independent of the characteristic length discussed above and governs the interpolation properties of the method. By default, the smoothing length is computed automatically. As the deformation progresses, particles move with respect to each other and, hence, the neighbors of a given particle can (and typically do) change. Every increment Abaqus/Explicit re-computes this local connectivity internally and computes kinematic quantities (such as normal and shear strains, deformation

gradients, etc.) based on contributions from this cloud of particles centered at the particle of interest. Stresses are then computed in a similar fashion as for reduced-integration brick elements, which are in turn used to compute element nodal forces for the particles in the cloud based on the smoothed particle hydrodynamic formulation.

By default, Abaqus/Explicit computes a smoothing length at the beginning of the analysis such that the average number of particles associated with an element is roughly between 30 and 50.

The smoothing length is kept constant during the analysis. Therefore, the average number of particles per element can either decrease or increase during the analysis depending on whether the average behavior in the model is expansive or compressive, respectively. If the analysis is mostly compressive in nature, the total number of particles associated with a given element might exceed the maximum allowed and the analysis will be stopped. By default, the maximum number of allowed particles associated with one element is 140.

12. Parameters tested and their effects:

Sr. No.	Criteria	Threshold	PPD	Kernel	Type of element	Second order accuracy	Output result
1	Strain	1	2		Hexagonal	Yes	solution did not converge
2	Strain	1.2	2	Cubic	Hexagonal	No	No conversion to particles
3	Strain	1.4	2	Cubic	Wedge	No	No conversion to particles
4	Strain	1.6	2	Cubic	Hexagonal	No	No conversion to particles
5	Strain	1.8	2	Cubic	Tetrahedron	No	No conversion to particles
6	Strain	2	2	Cubic	Hexagonal	No	No conversion to particles
7	Strain	2.2	2	Cubic	Hexagonal	No	No conversion to particles
8	Stress	1	3	Cubic	Wedge	No	No conversion to particles
9	Stress	1.2	4	Cubic	Hexagonal	No	No conversion to particles
10	Stress	1.4	5	Cubic	Tetrahedron	No	No conversion to particles
11	Time	1	2	Cubic	Hexagonal	No	No conversion to particles
12	Strain	1.00E-04	2	Cubic	Wedge	No	Conversion of particles
13	Strain	1.00E-05	3	Cubic	Hexagonal	No	Conversion of particles
14	Strain	1.00E-06	2	Cubic	Tetrahedron	No	Conversion of particles
15	Stress	0.0001	2	Cubic	Hexagonal	No	Conversion of particles
16	Stress	0.00001	3	Cubic	Wedge	No	Conversion of particles
17	Stress	0.000001	4	Cubic	Hexagonal	No	Conversion of particles
18	Stress	0.000001	5	Cubic	Tetrahedron	No	Conversion of particles
19	Time	0.0001	2	Cubic	Hexagonal	No	Conversion of particles
20	Time	0.00001	3	Cubic	Wedge	No	Conversion of particles
21	Time	0.000001	2	Cubic	Hexagonal	No	Conversion of particles
22	Time	0.0001	2	Cubic	Tetrahedron	No	Conversion of particles

Table: Different parameters tested for the conversion

These were the parameters which were tested by performing iterations and recording the results and its corresponding effects:

1) Having second order accuracy in the element control
2) Criteria
3) Particles per isoperimetric direction
4) Threshold value
5) Kernel Function
6) Type of element
7) The figure below shows the different parameters to decide the meshing element type and its conversion.

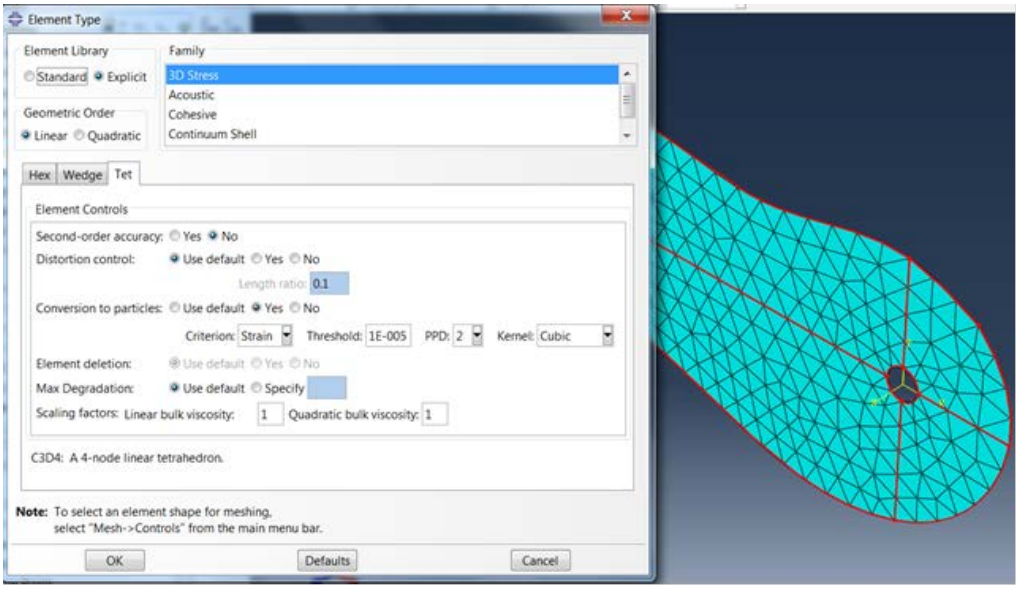

Figure:12.1- Showing various parameters for iterations:

So after trying out all of these different parameters the solution did converge and gave the results. But with these conversion of particles had no movement even after application of load.

13. **Boundary Conditions**:

The one far end of the body was fixed so that the part has the stability in the analysis and also that the solution should converge.

The second boundary condition being employed in this research is the ‘Displacement boundary condition’. This boundary condition gives the resulting movement of the particles on the application of the pressure on the inner surface of the cyst.

13.1. Boundary Condition in a Test model:

All the above iterations were done with a simple part i.e a long rectangular plate with a hole.

Where the plate represents the cross section of the nerve, the long plate is selected so as to minimize the effect of the fixed node and to have a fixed constrain over the body at the maximum possible distance. The hole represents the cyst with the objective to simulate the outward expansion resembling the expansion of a cyst.

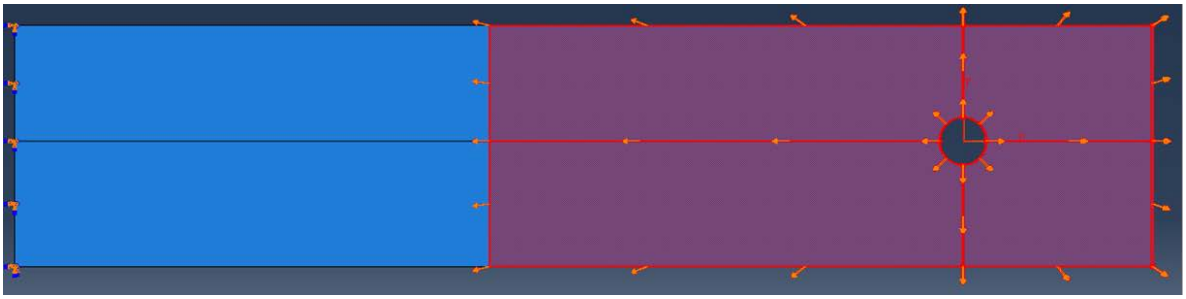

Figure: 13.1.1 – Plate with a hole:

Initially only a part of the long plate was selected to see the conversion to particles and the behavior of those particles during simulation.

So as we can see that on applying the strain criteria it has converted the domain to particles but the motion of the particles is not observed and as we can see it is the progressive strain to which the part is subjected and it spread gradually form the cyst to the neighboring region in the body.

Simulation with different criteria to check the motion of particle:

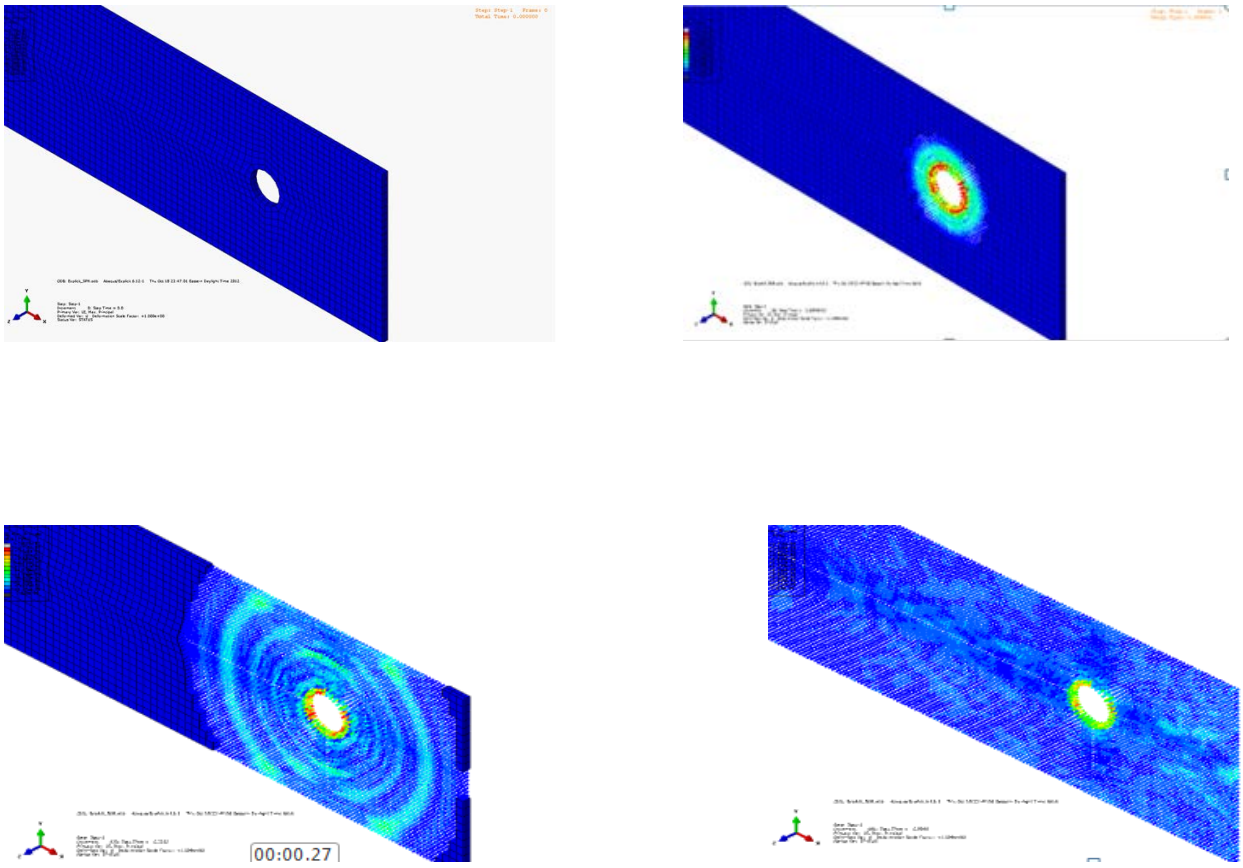

Figure: 13.1.1.-Strain Criteria

Applying the time criteria:

The time criteria is the time in seconds that we can specify for the analysis to convert the domain to particles. This criterion is generally effective in case where the time is a critical factor i.e the object is subjected to large deformation after certain time of the analysis. The example explained in the earlier section of a bird striking an aero-plane is a good example of the time criteria.

As you can see in the figure below the time criteria is successfully employed with the conversion of the particles but the particles still does not move with the analysis in progress. The conversion of particles observed in this simulation is not progressive but converts the entire domain to particles after attaining the specified time.

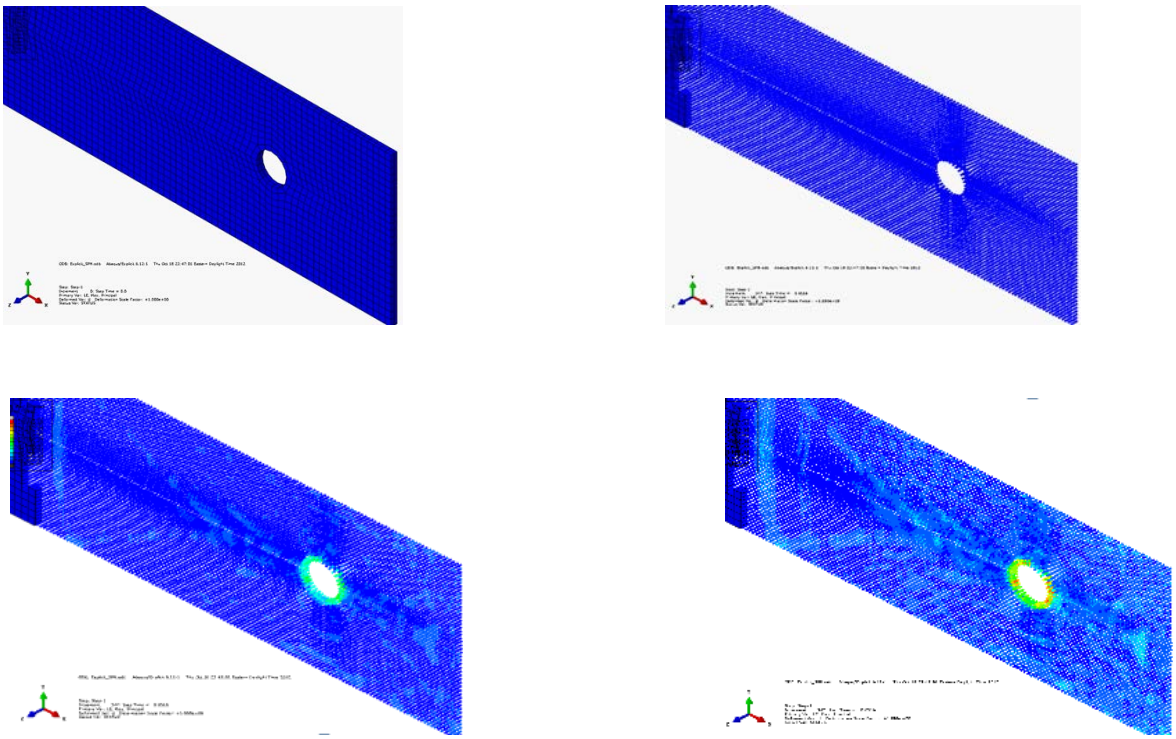

Figure: 13.1.2.-Time Criteria

After changing the static simulations to dynamic the movement of the particles was observed.

Initally the particles were tried with the displacement boundaru condition in the horizonatal direction and at the angle of 45 degrees since the boundary condition of the displacement of the particles was rectangular there was a need to change it to achieve the outward radial movement of the particles. Thus a new coordinate system; Cylindrical coordinate was defined only for the the second step i.e. the displacement boundary condition.

14. **RADIAL EXPANSION & ITS CONTROLLING PARAMETERS**:

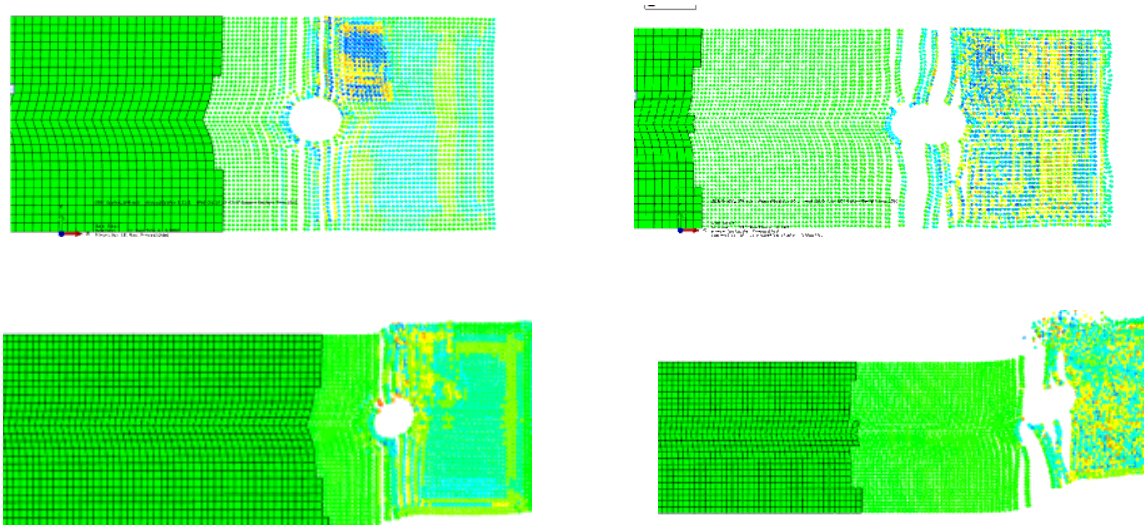

Figure: 14.1.- Horizontal movement of particles

Simulation shows the expansion of the cyst using cylindrical co-ordinate system. The change in system was a step to move towards the physical significance of the blow out of a cyst .

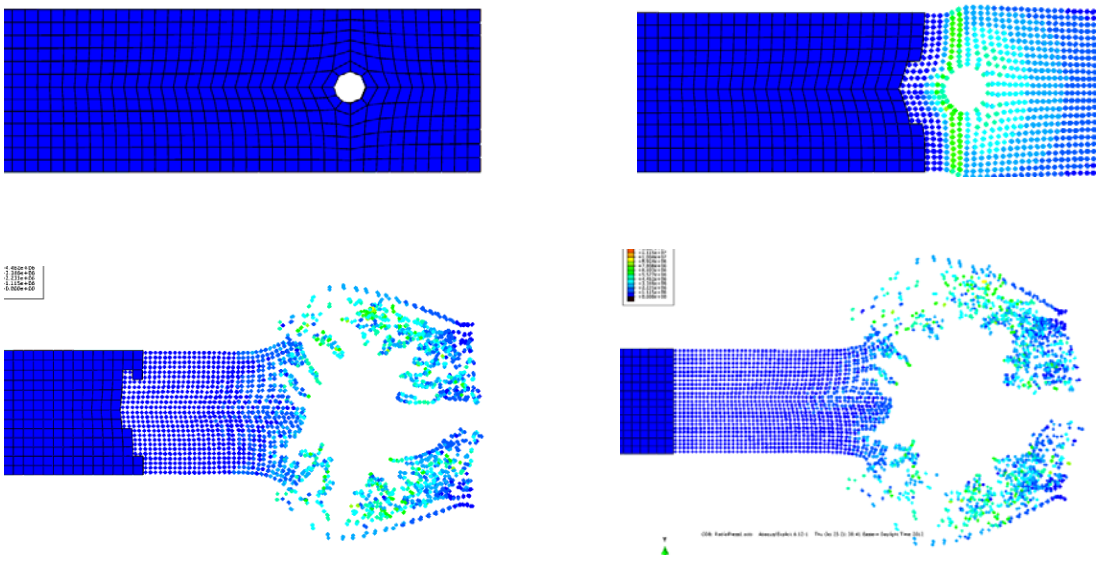

Figure: 14.2.-Particle movement in radial direction

Though the expansion in the radially outward direction was achieved but the motion of the particle was not in control and resembled more of an explosion than the gradual outward expansion of the cyst. Thus lot of iterations was done with the different parameters i.e. the time period, the steps for the simulation, the amplitude of the displacement etc. as shown in the figure.

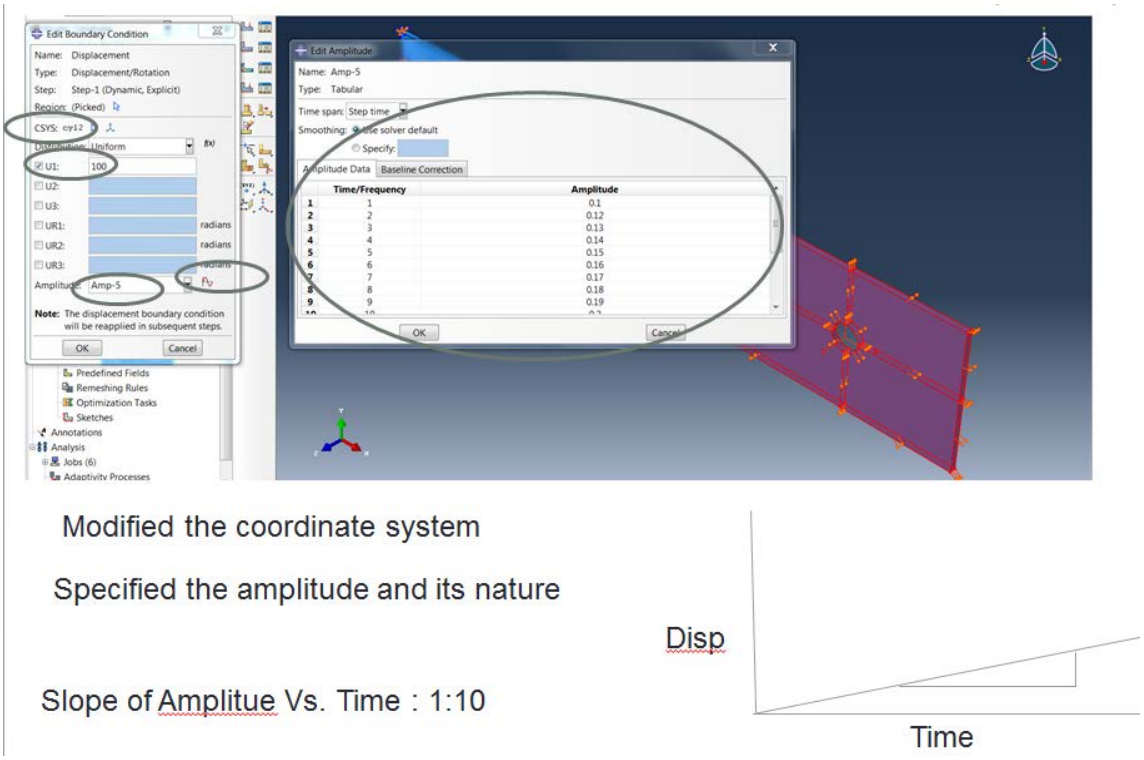

Figure: 14.3. - Optimizing Boundary Condition

Even after these iterations there were simulations which converted the nodes to particles and simulated the expansion but did not carry it though out the simulation. This was the time when the analysis was tested for the time period and the user defined steps of the solution , these user

defined steps were then again linked with the slope of the time and displacement graph which was an user input.

The figure below shows the simulation of one of these iterations :

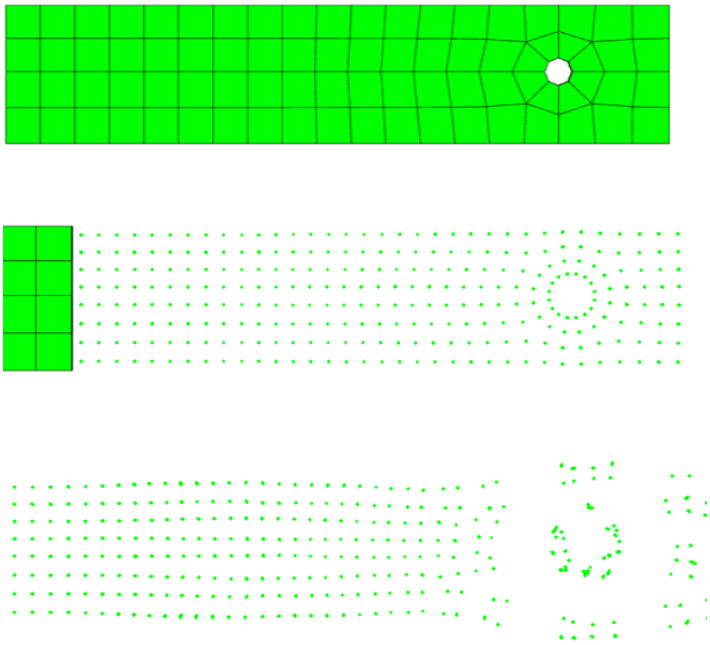

Figure: 14.4.- Simulation with different parameters

The control over the motion of the particle was thus finally achieved by finding a suitable relation between the times periods that is the total time for the simulation the time steps i.e. the time after which the displacement boundary condition is applied in stages and the nature of the time versus amplitude slope. It was observed that the best solution was achieved after having a comparatively long time period, shorter time steps and a gentle slope of the time and amplitude graph.

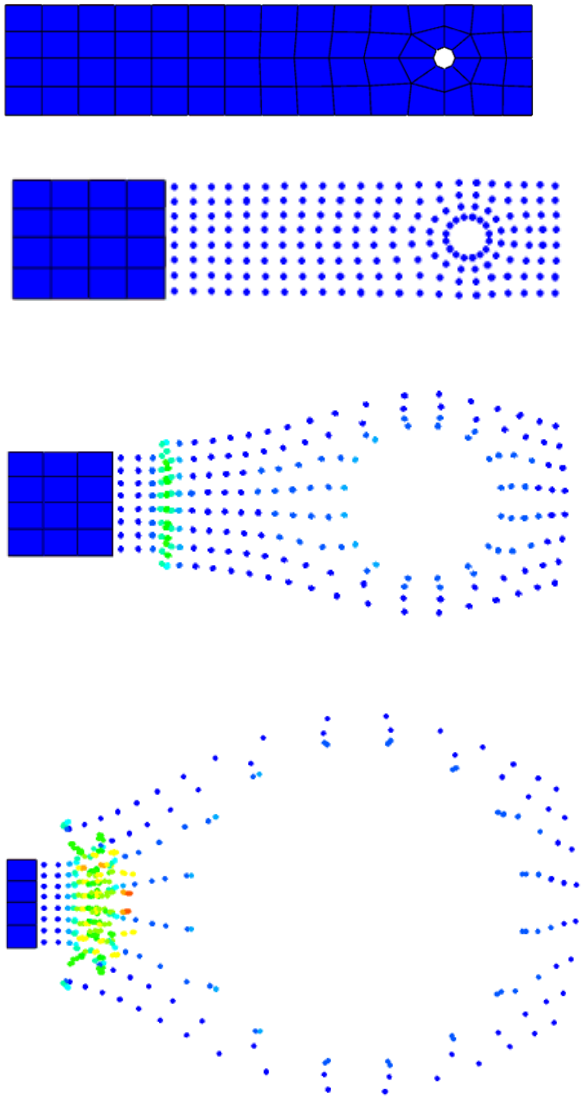

Figure: 14.5.-Controlled Particle Motion

Thus after this simulation it gave a confidence of using the SPH method of the large deformations. So a similar process was repeated with the changes as mentioned above for the cross section of a nerve. The figure below exhibits the slow and gradual expansion of the cyst.

15. **Implementation of SPH with the nerve cross section**:

This expansion of the cross section of the nerve is close to the physical blow out of a material having the elastic nature and capability to handle the large strain deformation.

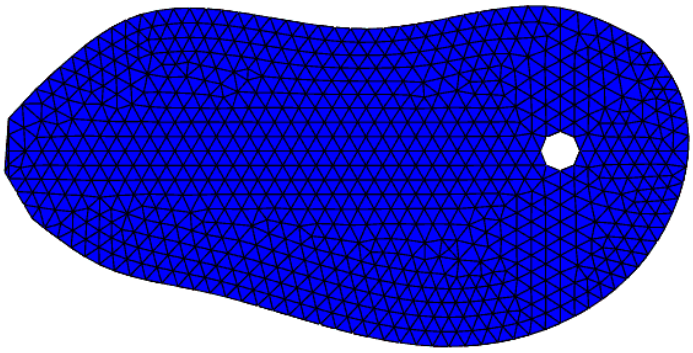

Figure: 15.1-Stage -1: This is the initial phase; body under the threshold strain value

After attaining the threshold limit the entire domain is gradually converted to particles

Figure: 15.2- Stage -2

Expansion of the cyst in the radially out ward direction:

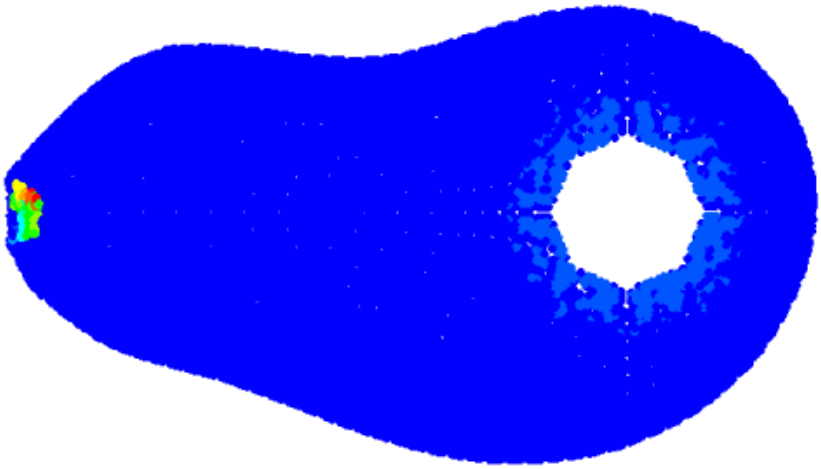

Figure: 15.3- Stage -3

The motion of the particle i.e. the circumference of the cyst and the Nerve cross section blowing outwards:

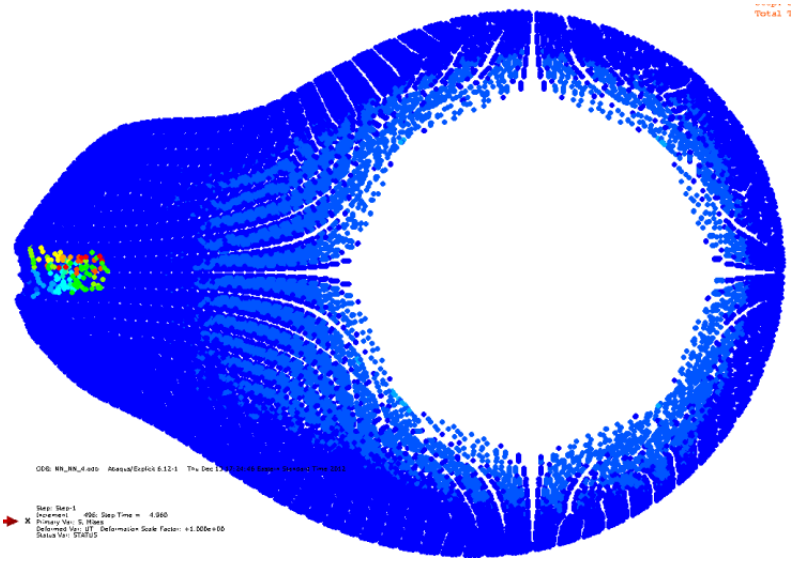

Figure: 15.4- Stage -4

16. Conclusion:

From the report we can conclude that the mesh-less method smoothed Hydrodynamic approach can be successfully applied to the Bio-medical applications like the expansion of a cyst.

The SPH method does give a solution for the large deformations where the conventional finite element methods are not capable of carrying the high strain deformations without distortion of nodes.

17. Future Scope:

The SPH method to be successfully applied to the 3D model biological organs

The SPH method should be capable of deciding the PPD as per the selection of the meshing element type and its size.

Analysis to be simulated considering the pressure exerted by the cystic fluid on the inner surface of the cyst involving pressure by incorporating the pressure boundary conditions in the SPH method.

18. References:

- Mesh Free Methods : Moving Beyond Finite Element method, By : G. R. Liu
- Abaqus release Notes : Abaqus 6.12
- International Journal of Rock Mechanics and Mining Sciences: Author: Shivkumar Karekal , Raj Das.
- SPH simulation of oil displacement in cavity-fracture structures: Author: Guangzheng Zhou, Zhihai Chen, Wei Ge
- Research Thesis : Puneet Soman ; 2012.